Turbulence-driven zonal flows in helical systems with radial electric fields

Turbulence-driven zonal flows in helical systems with radial electric fields

Cite as: Phys. Plasmas **16**, 056101 (2009); https://doi.org/10.1063/1.3077274
Submitted: 02 December 2008 • Accepted: 23 December 2008 • Published Online: 19 February 2009

H. Sugama and T.-H. Watanabe

Turbulence-driven zonal flows in helical systems with radial electric fields[a)]

H. Sugama[b)] and T.-H. Watanabe
National Institute for Fusion Science, Toki 509-5292, Japan and The Graduate University for Advanced Studies, Toki 509-5292, Japan

(Received 2 December 2008; accepted 23 December 2008; published online 19 February 2009)

Collisionless long-time responses of the zonal-flow potential to the initial condition and turbulence source in helical systems having radial electric fields are derived theoretically. All classes of particles in passing, toroidally trapped, and helical-ripple-trapped states are considered. The transitions between the toroidally trapped and helical-ripple-trapped states are taken into account while solving the gyrokinetic equation analytically by taking its average along the particle orbits. When the radial displacements of helical-ripple-trapped particles are reduced either by neoclassical optimization of the helical geometry lowering the radial drift or by strengthening the radial electric field E_r to boost the poloidal rotation, enhanced zonal-flow responses are obtained. Under the identical conditions on the magnitude of E_r and the magnetic geometry, using ions with a heavier mass gives rise to a higher zonal-flow response, and therefore the turbulent transport is expected to show a more favorable ion-mass dependence than the conventional gyro-Bohm scaling. © *2009 American Institute of Physics*. [DOI: 10.1063/1.3077274]

I. INTRODUCTION

It is widely accepted that zonal flows play a pivotal role in regulating turbulent transport in plasmas.[1,2] From the viewpoint of improving plasma confinement, it is important to investigate the magnetic configuration effects on turbulence-driven zonal flows. Theoretical studies on collisionless time evolution of zonal flows in tokamaks[3–6] and helical systems[7–12] such as heliotrons and stellarators elucidated how the zonal-flow response to a given turbulence source depends on the toroidal magnetic geometry that determines particle orbits. Our previous studies[7,8] predicted that the zonal-flow response can be increased in helical systems by reducing the radial drift velocities of helical-ripple-trapped particles. This implies that the helical configurations optimized for reducing neoclassical ripple transport[13–15] can simultaneously reduce the turbulent transport by enhancing the zonal-flow generation. In fact, the theoretical prediction was confirmed by the ion temperature gradient (ITG) turbulence simulation using the gyrokinetic Vlasov (GKV) code.[16–19] The simulation results agree with the confinement improvement that was observed experimentally in the inward-shifted plasma of the large helical device (LHD).[20,21] The reduction of anomalous transport by neoclassical optimization also provides an attractive scenario for improving plasma confinement in advanced helical configurations.[22–26]

In helical systems, the radial electric field E_r is produced from ambipolar particle fluxes[14] and it generates the macroscopic $\mathbf{E}\times\mathbf{B}$ rotation, which is distinguished from the microscopic sheared $\mathbf{E}\times\mathbf{B}$ zonal flows. The $\mathbf{E}\times\mathbf{B}$ rotation driven by E_r, which was not taken into account in our original theory,[7,8] is expected to reduce both neoclassical ripple transport and turbulent transport by improving the zonal-flow response.[10,18,19] In the zonal-flow theory by Mynick and Boozer,[10] the action-angle formalism is used to treat poloidally closed $\mathbf{E}\times\mathbf{B}$ drift orbits of helical-ripple-trapped particles as well as bounce orbits of toroidally trapped particles. However, for practical cases, such as in the LHD configuration, some helical-ripple-trapped particles cannot show poloidally closed orbits, and transitions between toroidally trapped and helical-ripple-trapped states can occur with some probability.[14,27] The effects of these transitions are included in this work to provide a comprehensive theory of zonal flows in helical systems. This paper provides new formulas, which we use to find how the helical geometry and E_r affect the collisionless time evolution of zonal flows. The E_r effects appear through the poloidal Mach number defined by $M_p \equiv |(cE_r/B_0r_0)(R_0q/v_{ti})|$ with the safety factor q, magnetic-field strength B_0, speed of light c, minor (major) radius r_0 (R_0), and ion thermal velocity $v_{ti}\equiv(T_i/m_i)^{1/2}$. Therefore, when the magnitude of E_r and the magnetic geometry are fixed, a higher zonal-flow response is obtained using ions with a heavier mass, which increases M_p, and accordingly the resultant turbulent transport is expected to show a more favorable ion-mass dependence than the conventional gyro-Bohm scaling.[28]

Basic equations describing zonal flows in helical systems are shown in Sec. II, and the analytical solutions of the distribution function are given in Sec. III, where we consider all classes of particle orbits and treat the transitions between the toroidally trapped and helical-ripple-trapped particles in the presence of the radial electric field E_r. In Sec. IV, the collisionless long-time zonal-flow responses to the initial condition and ITG turbulence are derived by including effects of the helical geometry and E_r. Finally, conclusions are given in Sec. V.

II. BASIC EQUATIONS

In this study, we consider the same helical magnetic configuration as in Ref. 8. We use the toroidal coordinates (r,θ,ζ), where r, θ, and ζ denote the flux-surface label, poloidal angle, and toroidal angle, respectively. The magnetic

[a)]Paper YI2 2, Bull. Am. Phys. Soc. **53**, 322 (2008).
[b)]Invited speaker.

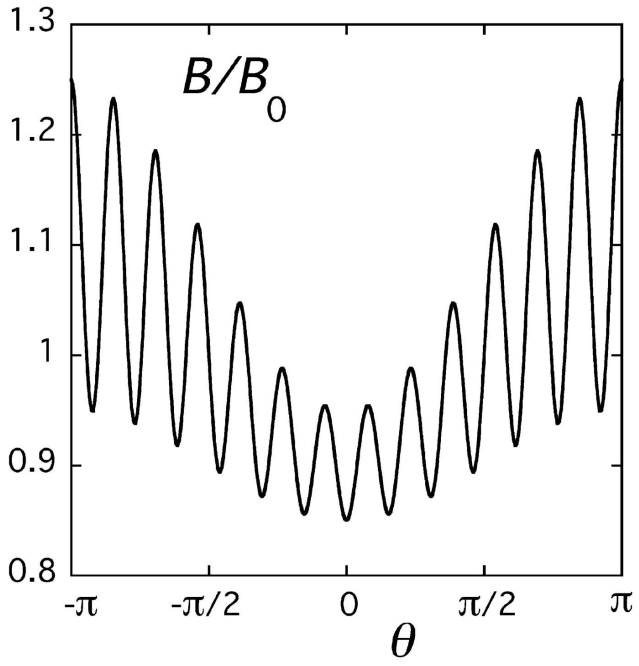

FIG. 1. An example of a profile of the magnetic-field strength along the field line ($\zeta=q\theta$). Here, $B/B_0=1-\epsilon_t\cos\theta-\epsilon_H(\theta)\cos(L\theta-M\zeta)$, $L=2$, $M=10$, $q=1.5$, $\epsilon_t=0.1$, and $\epsilon_H(\theta)=0.1\times(1-0.5\cos\theta)$ are used.

field is written as $\mathbf{B}=\nabla\psi(r)\times\nabla[\theta-\zeta/q(r)]$, where $2\pi\psi(r)$ is equal to the toroidal flux present within the flux surface labeled r, and $q(r)$ represents the safety factor. The magnetic-field strength is expressed by a function of the poloidal and toroidal angles (its r dependence is not shown here for simplicity) as[8,13]

$$B=B_0[1-\epsilon_T(\theta)-\epsilon_H(\theta)\cos\{L\theta-M\zeta+\chi_H(\theta)\}], \tag{1}$$

where M (L) is the toroidal (main poloidal) period number of the helical field. For the LHD, $L=2$ and $M=10$. Here, we assume that $L/(qM)\sim\epsilon_T\sim\epsilon_H\ll 1$. In this study, we set $\epsilon_T(\theta)=\epsilon_t\cos\theta$. Multiple-helicity effects from the Fourier components $\propto\cos\{(L+n)\theta-M\zeta\}$ with $n=\pm1,\pm2,\ldots$ can be included in the function $\epsilon_H(\theta)$,[8,13] which is even in θ and never takes negative values. An example of the profile of the field strength along the field line $\zeta=q\theta$ is shown in Fig. 1.

The gyrokinetic equation[29] for the zonal flow component with the perpendicular wave-number vector $\mathbf{k}_\perp=k_r\nabla r$ is given by

$$\left(\frac{\partial}{\partial t}+v_\parallel\mathbf{b}\cdot\nabla+i\omega_D+V_E\right)g_{\mathbf{k}_\perp}$$
$$=\frac{e}{T}F_0J_0(k_\perp\rho)\frac{\partial\phi_{\mathbf{k}_\perp}}{\partial t}+S_{\mathbf{k}_\perp}F_0, \tag{2}$$

where F_0 is the local equilibrium distribution function taking the Maxwellian form, $J_0(k_\perp\rho)$ is the zeroth-order Bessel function, $\rho=v_\perp/\Omega$ is the gyroradius, and $\Omega=eB/(mc)$ is the gyrofrequency. Here, the subscripts representing particle species are dropped for simplicity. The drift frequency ω_D is defined by $\omega_D\equiv\mathbf{k}_\perp\cdot\mathbf{v}_d\equiv k_rv_{\mathrm{dr}}$, where $v_{\mathrm{dr}}=\mathbf{v}_d\cdot\nabla r$ is the radial component of the gyrocenter drift velocity, and the radial coordinate r is defined by $\psi=B_0r^2/2$. The $\mathbf{E}\times\mathbf{B}$ drift velocity $\mathbf{v}_E\equiv(c/B)E_r\nabla r\times\mathbf{b}$ caused by the equilibrium radial electric field E_r is included in the differential operator $V_E\equiv\mathbf{v}_E\cdot\nabla$. In this study, we assume E_r to be constant. On the right-hand side of Eq. (2), the source term $S_{\mathbf{k}_\perp}F_0$ represents the $\mathbf{E}\times\mathbf{B}$ nonlinearity and is given by $S_{\mathbf{k}_\perp}F_0=(c/B)\Sigma_{\mathbf{k}'_\perp+\mathbf{k}''_\perp=\mathbf{k}_\perp}[\mathbf{b}\cdot(\mathbf{k}'_\perp\times\mathbf{k}''_\perp)]J_0(k'_\perp\rho)\phi_{\mathbf{k}'_\perp}g_{\mathbf{k}'_\perp}$. In Eq. (2), $g_{\mathbf{k}_\perp}$ is considered as a function of independent variables $(r,\theta,\zeta,\varepsilon,\mu)$, where $\varepsilon\equiv\frac{1}{2}mv^2+e\Phi$ and $\mu\equiv mv_\perp^2/(2B)$ represent the energy and magnetic moment of the particle, respectively. The gyrokinetic equation given in Eq. (2) is based on the ballooning representation[30] which is used to describe the local structure of perturbations with perpendicular wavelengths that are much smaller than the equilibrium scale lengths. We consider the local region around the magnetic surface $r=r_0$ and express the equilibrium electrostatic potential as $\Phi=-E_rx$, where $x\equiv r-r_0$.

As discussed in Ref. 18, although the potential fluctuation $\phi_{\mathbf{k}_\perp}$ producing zonal flows is constant on the flux surface, the solution $g_{\mathbf{k}_\perp}$ of Eq. (2) must have a dependence on the field line label $\alpha\equiv\zeta-q(r)\theta$ in helical systems, because ω_D depends on α. Then, $V_Eg_{\mathbf{k}_\perp}$ in Eq. (2) does not vanish, and it shows effects of the equilibrium radial electric field on $g_{\mathbf{k}_\perp}$ and accordingly affects behaviors of the zonal-flow potential. It is assumed in Eq. (2) that the components of grad B and curvature drift velocities parallel to $\nabla r\times\mathbf{b}$ are negligible compared with the magnitude of $\mathbf{v}_E$.

The perturbed *particle* distribution function $\delta f_{\mathbf{k}_\perp}$ is written in terms of the electrostatic potential $\phi_{\mathbf{k}_\perp}$ and the solution $g_{\mathbf{k}_\perp}$ of Eq. (2) as

$$\delta f_{\mathbf{k}_\perp}=-\frac{e\phi_{\mathbf{k}_\perp}}{T}F_0+g_{\mathbf{k}_\perp}e^{-i\mathbf{k}_\perp\cdot\boldsymbol{\rho}}, \tag{3}$$

where $\boldsymbol{\rho}=\mathbf{b}\times\mathbf{v}/\Omega$. The perturbed *gyrocenter* distribution function $\delta f^{(g)}_{\mathbf{k}_\perp}$ is given by

$$\delta f^{(g)}_{\mathbf{k}_\perp}=-J_0(k_\perp\rho)\frac{e\phi_{\mathbf{k}_\perp}}{T}F_0+g_{\mathbf{k}_\perp}. \tag{4}$$

The perturbed gyrocenter distribution function $\delta f^{(g)}_{\mathbf{k}_\perp}$ and the nonadiabatic part $g_{\mathbf{k}_\perp}$ are independent of the gyrophase although the perturbed particle distribution function $\delta f_{\mathbf{k}_\perp}$ depends on it as seen from the factor $e^{-i\mathbf{k}_\perp\cdot\boldsymbol{\rho}}$ on the right-hand side of Eq. (3). Using Eqs. (3) and (4), we obtain

$$\delta f_{\mathbf{k}_\perp}=\delta f^{(g)}_{\mathbf{k}_\perp}e^{-i\mathbf{k}_\perp\cdot\boldsymbol{\rho}}-\frac{e\phi_{\mathbf{k}_\perp}}{T}F_0[1-J_0(k_\perp\rho)e^{-i\mathbf{k}_\perp\cdot\boldsymbol{\rho}}]. \tag{5}$$

On the right-hand side of Eq. (5), the factor $e^{-i\mathbf{k}_\perp\cdot\boldsymbol{\rho}}$ of the first term arises from the difference between the particle and gyrocenter positions, while the second group of terms represents the classical polarization. The classical polarization refers to the variation of the particle distribution caused by the potential perturbation in the magnetized plasma where particles are subject to gyromotion around the field lines.

III. ANALYTICAL SOLUTION OF THE PERTURBED DISTRIBUTION FUNCTION

In this section, we solve the gyrokinetic equation in Eq. (2) analytically to obtain the perturbed distribution function for determining the long-time behavior of zonal flows. For that purpose, different classes of collisionless particle orbits are investigated.

Particles trapped in helical ripples are characterized by $\kappa^2<1$, where the trapping parameter κ is defined by

$$\kappa^2=\frac{\varepsilon-\mu B_0\{1-\epsilon_T(\theta)-\epsilon_H(\theta)\}+eE_rx}{2\mu B_0\epsilon_H(\theta)}. \tag{6}$$

Using the condition $L/(qM)\ll 1$, we approximate the field line element dl by $R_0d\zeta$, where R_0 denotes the major radius of the toroid. Then, the orbital average within a helical ripple is defined by

$$\bar{A}=\begin{cases}\dfrac{1}{2}\displaystyle\sum_{\sigma=\pm 1}\int_{\zeta_1}^{\zeta_2}(R_0d\zeta/|v_\parallel|)A \Big/ \int_{\zeta_1}^{\zeta_2}(R_0d\zeta/|v_\parallel|) & \text{for } \kappa^2<1\\ \displaystyle\int_{\zeta_0-\pi/M}^{\zeta_0+\pi/M}(R_0d\zeta/|v_\parallel|)A \Big/ \int_{\zeta_0-\pi/M}^{\zeta_0+\pi/M}(R_0d\zeta/|v_\parallel|) & \text{for } \kappa^2>1,\end{cases} \tag{7}$$

where $\sigma=v_\parallel/|v_\parallel|$ is the sign of the parallel velocity, (ζ_1,ζ_2) represents a toroidal-angle interval for a particle trapped within a helical ripple, and $(\zeta_0-\pi/M,\zeta_0+\pi/M)$ corresponds to a whole helical ripple around the local minimum of B at $\zeta=\zeta_0$. Using the longitudinal adiabatic invariant J (Refs. 13, 14, and 27) given by

$$J=\begin{cases}2\displaystyle\int_{\zeta_1}^{\zeta_2}R_0d\zeta|v_\parallel| & \text{for } \kappa^2<1\\ \displaystyle\int_{\zeta_0-\pi/M}^{\zeta_0+\pi/M}d\zeta\left(R_0|v_\parallel|-\sigma\frac{e\psi' x}{mcq}\right) & \text{for } \kappa^2>1\end{cases}=\begin{cases}16\dfrac{R_0}{M}\left(\dfrac{\mu B_0\epsilon_H}{m}\right)^{1/2}[E(\kappa)-(1-\kappa^2)K(\kappa)] & \text{for } \kappa^2<1\\ -\sigma\dfrac{2\pi}{M}\dfrac{e\psi' x}{mcq}+8\dfrac{R_0}{M}\left(\dfrac{\mu B_0\epsilon_H}{m}\right)^{1/2}\kappa E(\kappa^{-1}) & \text{for } \kappa^2>1,\end{cases} \tag{8}$$

and the time period τ_h given by

$$\tau_h=m\frac{\partial J(\varepsilon,\theta,x,\mu)}{\partial\varepsilon}=\begin{cases}2\displaystyle\int_{\zeta_1}^{\zeta_2}R_0d\zeta/|v_\parallel| & \text{for } \kappa^2<1\\ \displaystyle\int_{\zeta_0-\pi/M}^{\zeta_0+\pi/M}R_0d\zeta/|v_\parallel| & \text{for } \kappa^2>1\end{cases}=\begin{cases}4(R_0/M)(\mu B_0\epsilon_H/m)^{-1/2}K(\kappa) & \text{for } \kappa^2<1\\ 2(R_0/M)(\mu B_0\epsilon_H/m)^{-1/2}\kappa^{-1}K(\kappa^{-1}) & \text{for } \kappa^2>1,\end{cases} \tag{9}$$

along with the complete elliptic integrals $K(\kappa)$ and $E(\kappa)$, the orbital average of the radial drift velocity within a helical ripple is given by

$$\bar{v}_{dr}=\frac{mc}{e\psi'\tau_h}\frac{\partial J(\varepsilon,\theta,x,\mu)}{\partial\theta}=-\frac{c}{e\psi'}\frac{\partial H(\theta,x,\mu,J)}{\partial\theta}=\begin{cases}\dfrac{c\mu B_0}{e\psi'}\left[\dfrac{\partial\epsilon_H}{\partial\theta}\left\{\dfrac{2E(\kappa)}{K(\kappa)}-1\right\}+\dfrac{\partial\epsilon_T}{\partial\theta}\right] & \text{for } \kappa^2<1\\ \dfrac{c\mu B_0}{e\psi'}\left[\dfrac{\partial\epsilon_H}{\partial\theta}\left\{2\kappa^2\left(\dfrac{E(\kappa^{-1})}{K(\kappa^{-1})}-1\right)+1\right\}+\dfrac{\partial\epsilon_T}{\partial\theta}\right] & \text{for } \kappa^2>1,\end{cases} \tag{10}$$

where $\psi'=B_0r_0$. In a similar way, the averaged poloidal angular velocity ω_θ is expressed as

$$\omega_\theta=-\frac{mc}{e\psi'\tau_h}\frac{\partial J(\varepsilon,\theta,x,\mu)}{\partial x}=\frac{c}{e\psi'}\frac{\partial H(\theta,x,\mu,J)}{\partial x}=\begin{cases}-\dfrac{cE_r}{\psi'} & \text{for } \kappa^2<1\\ \dfrac{2\pi\sigma}{qM\tau_h}-\dfrac{cE_r}{\psi'} & \text{for } \kappa^2>1,\end{cases} \tag{11}$$

where the functions $J(\varepsilon,\theta,x,\mu)$ and $\varepsilon=H(\theta,x,\mu,J)$ are defined from substituting Eq. (6) into Eq. (8). The x dependencies of J and H are due to the term eE_rx present in Eq. (6), where the other x dependences in $\mu B_0(1-\epsilon_T-\epsilon_H)$ and $\mu B_0\epsilon_H$ are neglected. Therefore, the $\mathbf{E}\times\mathbf{B}$ drift appears in Eq. (11), but the grad B and curvature drifts do not appear.

The parallel derivative is rewritten as $\mathbf{b}\cdot\nabla\simeq R_0^{-1}(\partial/\partial\zeta+q^{-1}\partial/\partial\theta)$. Then, we use $(\partial g_{\mathbf{k}_\perp}/\partial\theta)/(\partial g_{\mathbf{k}_\perp}/\partial\zeta)\sim r_0/R_0\ll 1$ and $V_Eg_{\mathbf{k}_\perp}\simeq-(cE_r/B_0r_0)(\partial g_{\mathbf{k}_\perp}/\partial\theta)$ in Eq. (2). Moreover, we replace ω_D $(=k_rv_{dr})$ with $\bar{\omega}_D$ $(=k_r\bar{v}_{dr})$, which is justified because the radial displacement δ_r [see Eq. (26) in Ref. 8] of the gyrocenter from the helical-ripple-averaged radial position is much smaller than the gyroradius ρ for helical systems with $M\gg 1$. Based on these approximations, we obtain the lowest-order equation $(v_\parallel/R_0)(\partial g_{\mathbf{k}_\perp}/\partial\zeta)=0$ from Eq. (2),

where $\partial g_{\mathbf{k}_\perp}/\partial t$ is dropped because the long-time behavior of zonal flows with characteristic frequencies much smaller than $v_\parallel/(R_0 q)$ is considered. Therefore, to the lowest order, $g_{\mathbf{k}_\perp}$ is independent of ζ; hence, we write $g_{\mathbf{k}_\perp} \simeq \bar{g}_{\mathbf{k}_\perp} \equiv \bar{h}(x,\theta,\varepsilon,\mu)$. Here, the characteristic gradient scale length of h in the x direction is of the order of the equilibrium gradient scale length and the x dependence is distinguished from the rapid variation described by the factor $e^{ik_r x}$. The equation for h is derived from Eq. (2) by the averaging operation in Eq. (7) and is given as

$$\left(\frac{\partial}{\partial t} + \omega_\theta \frac{\partial}{\partial \theta} + ik_r \bar{v}_{\mathrm{dr}}\right) h = F_0 \overline{\left(J_0 \frac{e}{T}\frac{\partial \phi_{\mathbf{k}_\perp}}{\partial t} + S_{\mathbf{k}_\perp}\right)}. \tag{12}$$

In this work, we consider the case where the poloidal Mach number defined by $M_p \equiv |(cE_r/B_0 r_0)(R_0 q/v_t)|$ with $v_t \equiv (T/m)^{1/2}$ is much less than unity. Then, for particles with $\kappa^2 > 1$, which are not trapped in helical ripples, the contribution of parallel motion to the poloidal angular velocity ω_θ is much greater than that of the $\mathbf{E}\times\mathbf{B}$ drift, and therefore the E_r term in Eq. (11) for $\kappa^2 > 1$ is neglected. Now, for $\kappa^2 > 1$, Eq. (12) is rewritten as

$$\left(\frac{\partial}{\partial t} + \omega_\theta \frac{\partial}{\partial \theta}\right)(e^{ik_r \Delta_r} h) = e^{ik_r \Delta_r} F_0 \overline{\left(J_0 \frac{e}{T}\frac{\partial \phi_{\mathbf{k}_\perp}}{\partial t} + S_{\mathbf{k}_\perp}\right)}, \tag{13}$$

where h is regarded as a function of θ, ε, μ, and $\sigma \equiv v_\parallel/|v_\parallel|$. In Eq. (13),

$$\Delta_r(\theta,\varepsilon,\mu) = \sigma \frac{qM}{2\pi}\frac{mc}{e\psi'}[J(\varepsilon,\theta,\mu) - J_t(\varepsilon,\mu)] \quad (\text{for } \kappa^2 > 1) \tag{14}$$

represents the radial displacement of the helical-ripple-averaged gyrocenter position, and J_t is defined below. For $\kappa^2 > 1$, there are two types of particles, namely, particles trapped by toroidicity and passing particles. Figure 2(a) shows the (θ,κ^2) plane, where the regions for different classes of particles are divided by three boundary lines C_1, C_2, and C_3. In this figure, we consider the radial position $r = r_0$ (or $x=0$) and assume that the profile of the magnetic-field strength along the field line is similar to that in Fig. 1, where the maximum field strength B_M is given at $\theta = \pi$. Line C_1 is defined by $\kappa^2 = 1$, while C_2 is defined by Eq. (6) using $\varepsilon = \mu B_M \equiv \mu B_0[1 - \epsilon_T(\pi) + \epsilon_H(\pi)]$ ($x=0$ is assumed). Passing particles are defined by $\varepsilon > \mu B_M$, and they belong to the region above C_2. On the other hand, toroidally trapped particles are defined by $\varepsilon < \mu B_M$ with $\kappa^2 > 1$, and their region is bounded between C_1 and C_2. The trapping parameter κ^2 for $x=0$ is expressed as $\kappa^2 = \kappa^2(\lambda,\theta) \equiv [1 - \lambda B_0\{1 - \epsilon_T(\theta) - \epsilon_H(\theta)\}]/[2\lambda B_0 \epsilon_H(\theta)]$, where $\lambda = \mu/\varepsilon$. Note that κ^2 is an even function of θ. Toroidally trapped particles, which have two invariants, ε and μ, reach the boundary line C_1 at poloidal angles $\theta = \pm\theta_t(\lambda)$. The angle $\theta_t(\lambda)$ is determined using the condition $\kappa^2[\lambda,\theta_t(\lambda)] = 1$ and $\theta_t(\lambda) \geq 0$. Now, J_t in Eq. (14) is defined by $J_t(\varepsilon,\mu) = J[\theta_t(\mu/\varepsilon),\varepsilon,\mu]$ for toroidally trapped particles and by $J_t(\varepsilon,\mu) = J(\pi,\varepsilon,\mu)$ for passing particles.

For particles with $\kappa^2 < 1$, which are trapped in helical ripples, it is convenient to use J instead of ε as one of the phase-space coordinates for representing h. Considering the radial position $x=0$ again, the energy variable ε is expressed as

$$\begin{aligned}\varepsilon &= W(\theta,J,\mu)\\ &\equiv H(\theta,x=0,\mu,J)\\ &\equiv \mu B_0[1 - \epsilon_T(\theta) + \epsilon_H\{2\kappa^2(\theta,J,\mu) - 1\}],\end{aligned} \tag{15}$$

where $\kappa^2(\theta,J,\mu)$ is implicitly defined using Eq. (8) for $\kappa^2 < 1$. As an approximate solution of Eq. (8) for κ^2 in the region $0 \leq \kappa^2 < 1$, we obtain

$$\kappa^2(\theta,J,\mu) \simeq C_\kappa X(\theta,J,\mu) - (C_\kappa - 1)[X(\theta,J,\mu)]^2, \tag{16}$$

where $X(\theta,J,\mu) \equiv J/[16(R_0/M)\{\mu B_0 \epsilon_H(\theta)/m\}^{1/2}]$. The dimensionless numerical coefficient C_κ in Eq. (16) is given as $C_\kappa = 1.329\,84$ by the least-mean-squares method. Equation (16) is useful when we need an explicit form of $W(\theta,J,\mu)$ of Eq. (15). Using Eqs. (10) and (11), we find

$$\begin{aligned}&\left(\omega_\theta \frac{\partial}{\partial \theta} + ik_r \bar{v}_{\mathrm{dr}}\right) h(\theta,J,\mu)\\ &\quad = \left(\omega_\theta \frac{\partial}{\partial \theta} + ik_r \bar{v}_{\mathrm{dr}} + eE_r \bar{v}_{\mathrm{dr}} \frac{\partial}{\partial \varepsilon}\right) h(\theta,\varepsilon,\mu).\end{aligned} \tag{17}$$

On the right-hand side of Eq. (17), the last term is regarded as negligible compared with the second term because of the

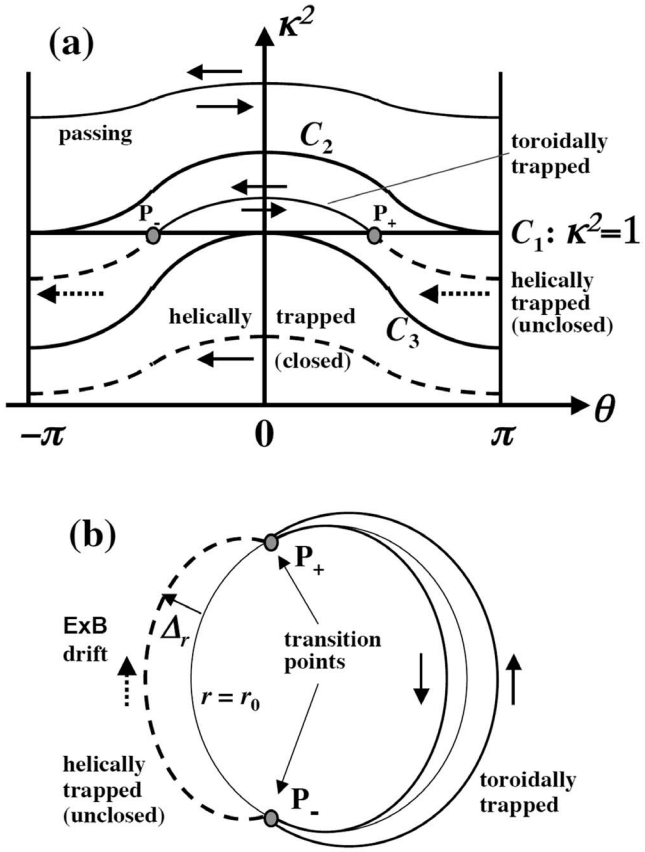

FIG. 2. (a) Particle orbits in the (θ,κ^2) plane and (b) poloidal cross sections of toroidally trapped and helically trapped orbits, between which transitions can occur. Dashed lines represent bounce-center $\mathbf{E}\times\mathbf{B}$ drift motions of helically trapped particles. Transition points P_+ and P_- are located at poloidal angles $\theta = \theta_t$ and $-\theta_t$, respectively.

order estimation $eE_r\partial/\partial\epsilon \sim e\Phi/(rT) \ll k_r$. Now, for $\kappa^2 < 1$, Eq. (12) is rewritten in a form similar to Eq. (13) as

$$\left(\frac{\partial}{\partial t} + \omega_\theta \frac{\partial}{\partial \theta}\right)[e^{ik_r\Delta_r} h_0(\theta, J, \mu)] = e^{ik_r\Delta_r} F_0 \overline{\left(J_0 \frac{e}{T}\frac{\partial \phi_{\mathbf{k}_\perp}}{\partial t} + S_{\mathbf{k}_\perp}\right)}, \tag{18}$$

where J is used as an independent variable instead of ε in Eq. (13), and the radial displacement of the bounce center of the helical-ripple-trapped particle is written as

$$\Delta_r(\theta, J, \mu) = \frac{1}{eE_r}[W(\theta, J, \mu) - W_t(J, \mu)] \quad (\text{for } \kappa^2 < 1), \tag{19}$$

where $W(\theta, J, \mu)$ is given by Eq. (15), while $W_t(J, \mu)$ is defined below. As shown in Fig. 2(a), the particle region $\kappa^2 < 1$ is divided by the curve C_3 into two regions. Here, the equation defining C_3 is obtained by substituting $J = J_c(\mu) \equiv 16(R/M)(\mu B_0 \epsilon_{H0}/m)^{1/2}$ into the left-hand side of Eq. (8) for $\kappa^2 < 1$, where $\epsilon_{H0} = \epsilon_H(0)$ in the case of Fig. 2(a). In the region below the curve C_3 where $J < J_c(\mu)$, the bounce centers of helical-ripple-trapped particles can show poloidally closed orbits, while in the region between C_1 and C_3, where $\kappa^2 < 1$ and $J > J_c(\mu)$, the bounce centers show poloidal drifts only in the bounded poloidal regions $[|\theta| > \theta_t$ in the case of Fig. 2(a)]. In Fig. 2(a), two points, P_+ and P_-, are located at the boundary poloidal angles, $\theta = \theta_t$ and $-\theta_t$, respectively. Here, θ_t can be expressed as a function of (J, μ), $\theta_t = \theta_t(J, \mu)$, which is derived from the relation obtained by taking the limit $\kappa^2 \to 1$ in Eq. (8) for $\kappa^2 < 1$. Now, W_t in Eq. (19) is defined as $W_t(J, \mu) = W[\theta_t(J, \mu), J, \mu]$ for $J > J_c(\mu)$ and as $W_t(J, \mu) = W(0, J, \mu)$ for $J < J_c(\mu)$.

Note that, on the boundary line $C_1(\kappa^2 = 1)$, particles can undergo transitions between the toroidally trapped and helical-ripple-trapped states. Figure 2(b) shows the poloidal cross sections of toroidally trapped and helically trapped orbits, between which transitions can occur. In Figs. 2(a) and 2(b), where $E_r > 0$ is assumed, both toroidally trapped particles with $v_\parallel > 0$ and helical-ripple-trapped particles undergo the transition to toroidally trapped particles with $v_\parallel < 0$ at point P_+ where $\theta = \theta_t$. On the other hand, at point P_-, where $\theta = -\theta_t$, toroidally trapped particles with $v_\parallel < 0$ change the sign of $v_\parallel$ or make the transition to helical-ripple-trapped particles. Although $E_r > 0$ is assumed throughout this work, we can treat the case of $E_r < 0$ in the same manner by noting that the transition from the toroidally trapped state with $v_\parallel > 0$ to the helically trapped state occurs at P_+ for $E_r < 0$. Using the theory by Cary *et al.*,[14,27] the probability P_t of the transition from the toroidally trapped $(v_\parallel < 0)$ to helical-ripple-trapped particles at P_- is given by

$$P_t = \left[\frac{(\partial J_{r0}/\partial x)(\partial \varepsilon_x/\partial \theta) - (\partial J_{r0}/\partial \theta)(\partial \varepsilon_x/\partial x)}{(\partial J_{-0}/\partial x)(\partial \varepsilon_x/\partial \theta) - (\partial J_{-0}/\partial \theta)(\partial \varepsilon_x/\partial x)}\right]_{\theta=-\theta_t}, \tag{20}$$

where

$$J_{r0} \equiv \lim_{\kappa^2 \to 1-0} J,$$

$$J_{-0} \equiv \lim_{\kappa^2 \to 1+0} J(\sigma = -1), \tag{21}$$

$$\varepsilon_x \equiv \mu B_0[1 - \epsilon_T(\theta) + \epsilon_H(\theta)] - eE_r x.$$

We note that the fractional expression within the brackets $[\cdots]$ at the right-hand side of Eq. (20) is an even function of θ; therefore, it takes the same value at $\theta = \theta_t$ and $-\theta_t$. Now, using Eqs. (8), (20), and (21), we obtain

$$P_t \simeq \frac{4\sqrt{2}}{\pi} M_p \left(\frac{v}{v_t}\right)^{-1} \left[\epsilon_H^{-1/2} \frac{\partial \epsilon_H/\partial \theta}{\partial(\epsilon_H - \epsilon_T)/\partial \theta}\right]_{\theta=\theta_t}. \tag{22}$$

Here, we find that $P_t \ll 1$ due to the smallness of M_p. Although $P_t \ll 1$, the average time duration spent by particles in the helically trapped state is comparable to that in the toroidally trapped state, because the poloidal angular velocity ω_θ is lower for the former state than for the latter by a factor proportional to $M_p (\ll 1)$. For the particles [in the regions between C_2 and C_3 in Fig. 2(a)] undergoing transitions, we define the average poloidal time period τ_{po} by

$$\tau_{\text{po}} \equiv \sum_{\sigma=\pm 1}\left[H(-\sigma)\int_{|\theta|<\theta_t} \frac{d\theta}{|\omega_\theta|} + H(\sigma)(1 - P_t)\int_{|\theta|<\theta_t} \frac{d\theta}{|\omega_\theta|}\right] + P_t \int_{|\theta|>\theta_t} \frac{d\theta}{|\omega_\theta|} \simeq \oint \frac{d\theta}{|\omega_\theta|}[2H(\kappa^2 - 1) + P_t H(1 - \kappa^2)] \tag{23}$$

and the poloidal-orbit average of an arbitrary function A for the toroidally trapped and helically trapped orbits by

$$\langle A \rangle_{\text{po}} \equiv \frac{1}{\tau_{\text{po}}} \sum_{\sigma=\pm 1}\left[H(-\sigma)\int_{|\theta|<\theta_t} \frac{A d\theta}{|\omega_\theta|} + H(\sigma)(1 - P_t)\int_{|\theta|<\theta_t} \frac{A d\theta}{|\omega_\theta|}\right] + P_t \int_{|\theta|>\theta_t} \frac{A d\theta}{|\omega_\theta|} \simeq \frac{1}{\tau_{\text{po}}}\oint \frac{d\theta}{|\omega_\theta|}\left[H(\kappa^2 - 1)\sum_{\sigma=\pm 1} A + H(1 - \kappa^2) P_t A\right], \tag{24}$$

where H is the Heaviside step function $[H(x) = 1$ for $x > 0$ and 0 for $x < 0]$ and $\sigma \equiv v_\parallel/|v_\parallel|$. Also, recall that $\omega_\theta = -cE_r/(B_0 r_0)$ for $\kappa^2 < 1$ and $2\pi\sigma/(qM\tau_h)$ for $\kappa^2 > 1$. When the transition occurs at $C_1(\kappa^2 = 1)$, the independent variable J for A in the helical-ripple-trapped state and the independent variable ε for A in the toroidally trapped state are connected to each other by the relation that is defined by substituting $\theta = \theta_t(\lambda)$ and $\lambda = \mu/\varepsilon$ into Eq. (15) as

$$\varepsilon = W[\theta_t(\mu/\varepsilon), J, \mu]. \tag{25}$$

Based on the operation defined in Eq. (24), the function A is

averaged over the connected orbits containing both parts of toroidally trapped and helical-ripple-trapped states so that $\langle A\rangle_{\rm po}$ is independent of θ and is regarded as a function of either (ε,μ) or (J,μ), where ε and J are related to each other by Eq. (25).

For passing particles [in the region above C_2 in Fig. 2(a)] and helical-ripple-trapped particles showing poloidally closed orbits (below C_3), $\tau_{\rm po}$ and $\langle A\rangle_{\rm po}$ are given by

$$\tau_{\rm po}\equiv\oint\frac{d\theta}{|\omega_\theta|}\quad\text{and}\quad\langle A\rangle_{\rm po}\equiv\frac{1}{\tau_{\rm po}}\oint\frac{Ad\theta}{|\omega_\theta|},\tag{26}$$

respectively.

This work is concerned with the long-time behavior of zonal flows, and the characteristic time scale is assumed to be much longer than $1/\omega_\theta$. To the lowest order, Eqs. (13) and (18) are both written in the same form as $\omega_\theta\partial(e^{ik_r\Delta_r}h)/\partial\theta=0$, implying that $e^{ik_r\Delta_r}h$ is independent of θ. Here, it should be noted that ε is used as an independent variable of h for $\kappa^2>1$, while J is used for $\kappa^2<1$. Then, using the poloidal-orbit average [defined in Eqs. (24) and (26)], integrating Eqs. (13) and (18) with respect to time, and using Eq. (4) with $g_{\mathbf{k}_\perp}\simeq\bar{g}_{\mathbf{k}_\perp}\equiv h$, we obtain

$$\begin{aligned}\langle e^{ik_r\Delta_r}h(t)\rangle_{\rm po}&=\langle e^{ik_r\Delta_r}[h(0)+F_0\overline{R_{\mathbf{k}_\perp}(t)}]\rangle_{\rm po}\\&\quad+\frac{e}{T}F_0\langle e^{ik_r\Delta_r}\overline{J_0\{\phi_{\mathbf{k}_\perp}(t)-\phi_{\mathbf{k}_\perp}(0)\}}\rangle_{\rm po}\\&=\langle e^{ik_r\Delta_r}\overline{[\delta f^{(g)}_{\mathbf{k}_\perp}(0)+F_0R_{\mathbf{k}_\perp}(t)]}\rangle_{\rm po}\\&\quad+\frac{e}{T}F_0\langle e^{ik_r\Delta_r}\overline{J_0\phi_{\mathbf{k}_\perp}(t)}\rangle_{\rm po},\end{aligned}\tag{27}$$

where $R_{\mathbf{k}_\perp}(t)\equiv\int_0^t S_{\mathbf{k}_\perp}(t')dt'$. The Appendix shows the derivation of Eq. (27) in detail. Equation (27) is valid for all passing, toroidally trapped, and helical-ripple-trapped states, although we should regard Δ_r and $\langle\cdots\rangle_{\rm po}$ in Eq. (27) as functions of (ε,μ) for $\kappa^2>1$ and of (J,μ) for $\kappa^2<1$. For regions between C_1 and C_3 in Fig. 2(a), where the transitions occur at $C_1(\kappa^2=1)$, ε and J are related to each other by Eq. (25). Now, using Eqs. (3) and (27), the perturbed particle distribution function is expressed in the identical form for all classes of particles as

$$\begin{aligned}\delta f_{\mathbf{k}_\perp}(t)&=-\frac{e}{T}\phi_{\mathbf{k}_\perp}(t)F_0[1-e^{-i\mathbf{k}_\perp\cdot\boldsymbol{\rho}}e^{ik_r\Delta_r}\langle e^{ik_r\Delta_r}\overline{J_0}\rangle_{\rm po}]\\&\quad+e^{-i\mathbf{k}_\perp\cdot\boldsymbol{\rho}}e^{-ik_r\Delta_r}\langle e^{ik_r\Delta_r}\overline{[\delta f^{(g)}_{\mathbf{k}_\perp}(0)+F_0R_{\mathbf{k}_\perp}(t)]}\rangle_{\rm po},\end{aligned}\tag{28}$$

where $\phi_{\mathbf{k}_\perp}=\langle\phi_{\mathbf{k}_\perp}\rangle$ is used. At the right-hand side of Eq. (28), the first group of terms proportional to $\phi_{\mathbf{k}_\perp}(t)$ represents the classical and neoclassical polarizations due to gyromotion and drift motion of particles, while the second group of terms represents the initial condition and the turbulent source.

IV. COLLISIONLESS LONG-TIME ZONAL-FLOW RESPONSE IN THE PRESENCE OF THE EQUILIBRIUM ELECTRIC FIELD

To determine the zonal-flow potential, we use Poisson's equation written as

$$\int d^3v\,\delta f_{i\mathbf{k}_\perp}-\int d^3v\,\delta f_{e\mathbf{k}_\perp}=n_0\frac{e\phi_{\mathbf{k}_\perp}}{T_e}(k_\perp\lambda_{\rm De})^2,\tag{29}$$

where the subscripts representing ions (i) and electrons (e) are shown explicitly, and $\lambda_{\rm De}\equiv[T_e/(4\pi n_0e^2)]^{1/2}$ is the electron Debye length. Then, substituting Eq. (28) into Eq. (29) and taking its flux-surface average, we obtain

$$\frac{e\phi_{\mathbf{k}_\perp}(t)}{T_i}=\frac{\langle I(t)\rangle}{\mathcal{D}},\tag{30}$$

which describes the collisionless long-time behavior of the zonal-flow potential. Here, $\langle\cdots\rangle$ denotes the flux-surface average, and the shielding effects are represented by

$$\begin{aligned}\mathcal{D}&=\sum_{a=i,e}\frac{T_i}{T_a}\left\langle\int d^3vF_{a0}[1-|\langle e^{ik_r\Delta_{ar}}\overline{J_0(k_\perp\rho_a)}\rangle_{\rm po}|^2]\right\rangle\\&\quad+n_0(T_i/T_e)(k_\perp\lambda_{\rm De})^2,\end{aligned}\tag{31}$$

while the initial conditions and nonlinear sources are included in

$$\begin{aligned}\langle I(t)\rangle&=\sum_{a=i,e}\frac{e_a}{e}\left\langle\int d^3vJ_0(k_\perp\rho_a)e^{-ik_r\Delta_{ar}}\right.\\&\quad\left.\times\langle e^{ik_r\Delta_{ar}}\overline{[\delta f^{(g)}_{a\mathbf{k}_\perp}(0)+F_{a0}R_{a\mathbf{k}_\perp}(t)]}\rangle_{\rm po}\right\rangle.\end{aligned}\tag{32}$$

Note that Eqs. (30)–(32) can be applied to the zonal-flow potential for wide wave-number ranges, including both ITG and electron temperature gradient turbulences.

Now, we consider the wave-number region relevant to the ITG turbulence, where $k_\perp\rho_i<1$, and take the small-electron-gyroradius limit $k_\perp\rho_e\to0$. In this case, we also have $k_\perp\lambda_{\rm De}\to0$, and Eq. (29) is reduced to the quasineutrality condition. Here, we also assume the radial displacement of ions to be so small that $k_r\Delta_{ir}<1$. Then, we use $k_r\Delta_{er}\to0$ for $\kappa^2>1$, where $\Delta_{er}\ll\Delta_{ir}$ because of the small electron gyroradius, while electrons and ions in the helical-ripple-trapped states $\kappa^2<1$, for which $\bar{v}_{{\rm dr}e}\sim\bar{v}_{{\rm dr}i}$, undergo radial displacements of the same order of magnitude, $\Delta_{er}\sim\Delta_{ir}$. Then, Eqs. (31) and (32) are expanded in terms of $k_\perp\rho_i$ and $k_r\Delta_{ir}$ to yield

$$\begin{aligned}\mathcal{D}&=n_0\langle k_\perp^2\rho_{ti}^2\rangle+\sum_{a=i,e}\frac{T_i}{T_a}\left\langle\int d^3vF_{a0}k_r^2\{\langle\Delta_{ar}^2\rangle_{\rm po}-\langle\Delta_{ar}\rangle_{\rm po}^2\}\right\rangle\\&=n_0\langle k_\perp^2\rho_{ti}^2\rangle[1+G_p+G_t+M_p^{-2}(G_{ht}+G_h)(1+T_e/T_i)]\end{aligned}\tag{33}$$

and

$$\langle I(t)\rangle = \left\langle \int d^3v[1 + ik_r\{\Delta_{ir} - \langle\Delta_{ir}\rangle_{\rm po}\}] \times \overline{[\delta f^{(g)}_{i\mathbf{k}_\perp}(0) + F_{i0}R_{i\mathbf{k}_\perp}(t)]} \right\rangle, \tag{34}$$

respectively, where $\rho_{ti} \equiv (T_i/m_i)^{1/2}/\Omega_i$ denotes the ion thermal gyroradius, and the contribution of electrons to $\langle I(t)\rangle$ is neglected. The part proportional to T_e/T_i in Eq. (33) represents the contributions from electrons trapped in helical ripples. The dimensionless geometrical factors G_p, G_t, G_{ht}, and G_h in Eq. (33) are defined by

$$G_p = \frac{12}{\pi^3}B_0R_0^2q^2\left\langle\frac{B^2}{|\nabla\psi|^2}\right\rangle \times\int_0^{1/B_M} d\lambda\oint\frac{d\theta}{2\pi}(2\lambda B_0\epsilon_H)^{-1/2}\kappa^{-1}K(\kappa^{-1}) \times\left\{(2\lambda B_0\epsilon_H)^{1/2}\kappa E(\kappa^{-1}) - \frac{\oint\frac{d\theta}{2\pi}K(\kappa^{-1})E(\kappa^{-1})}{\oint\frac{d\theta}{2\pi}(2\lambda B_0\epsilon_H)^{-1/2}\kappa^{-1}K(\kappa^{-1})}\right\}^2,$$

$$G_t = \frac{3}{\pi^3}B_0\left(\frac{R_0q}{r_0}\right)^2\int_{1/B_M}^{1/B'_m}\hat{\tau}_{\rm po}(\lambda)d\lambda\langle H(\kappa^2-1) \times\{[\epsilon_H(\theta)]^{1/2}\kappa E(\kappa^{-1}) - \{\epsilon_H[\theta_t(\lambda)]\}^{1/2}\}^2\rangle_{\rm po},$$

$$G_{ht} = \frac{15}{32\pi}B_0\left(\frac{R_0q}{r_0}\right)^2\int_{1/B_M}^{1/B'_m}\hat{\tau}_{\rm po}(\lambda)d\lambda[\langle H(1-\kappa^2) \times\{\epsilon_*(\theta,\lambda)\}^2\rangle_{\rm po} - \langle H(1-\kappa^2)\epsilon_*(\theta,\lambda)\rangle^2_{\rm po}],$$

$$G_h = \frac{15}{\sqrt{2}\pi}\left(\frac{R_0q}{r_0}\right)^2(\epsilon_{H0})^{1/2}\Big[\langle(\widetilde{\epsilon_T} + \widetilde{\epsilon_H})^2\rangle_{\rm po} - 2C_\kappa(\epsilon_{H0})^{1/2}\langle\widetilde{(\epsilon_H)^{1/2}}(\widetilde{\epsilon_T} + \widetilde{\epsilon_H})\rangle_{\rm po} + \frac{4}{3}C_\kappa^2\epsilon_{H0}\langle\{\widetilde{(\epsilon_H)^{1/2}}\}^2\rangle_{\rm po}\Big], \tag{35}$$

where B_M denotes the maximum field strength over the flux surface, and B'_m represents the minimum value of the local maximum field strengths within each helical ripple. For Fig. 1, $B_M = B_0[1-\epsilon_T(\pi)+\epsilon_H(\pi)]$ and $B'_m = B_0[1-\epsilon_T(0)+\epsilon_H(0)]$. Here, G_p and G_t are related to passing and toroidally trapped particle orbits, respectively, while G_h and G_{ht} originate from the poloidally closed and unclosed orbits of helical-ripple-trapped particles, respectively. Integrals of functions of λ and θ must be calculated to determine these geometrical factors in Eq. (35), where $\hat{\tau}_{\rm po}(\lambda)$ and $\epsilon_*(\theta,\lambda)$ are defined by

$$\hat{\tau}_{\rm po}(\lambda) \equiv \frac{v\tau_{\rm po}}{R_0q} \equiv 4\sqrt{2}\oint\frac{d\theta}{2\pi}\Big(H(\kappa^2-1) \times\{\epsilon_H(\theta)\}^{-1/2}\kappa^{-1}K(\kappa^{-1}) + 2H(1-\kappa^2) \times\left[\epsilon_H^{-1/2}\frac{\partial\epsilon_H/\partial\theta}{\partial(\epsilon_H-\epsilon_T)/\partial\theta}\right]_{\theta=\theta_t}\Big) \tag{36}$$

and

$$\epsilon_*(\theta,\lambda) = \epsilon_T(\theta) + \epsilon_H(\theta) - 2C_\kappa\{\epsilon_T(\theta)\epsilon_H[\theta_t(\lambda)]\}^{1/2} + (2C_\kappa - 1)\epsilon_H[\theta_t(\lambda)] - \epsilon_T[\theta_t(\lambda)], \tag{37}$$

respectively. The poloidal-angle functions $\widetilde{\epsilon_T}$, $\widetilde{\epsilon_H}$, and $\widetilde{(\epsilon_H)^{1/2}}$, which are used to define G_h, are given by

$$\widetilde{\epsilon_T} = \epsilon_T - \langle\epsilon_T\rangle_{\rm po}, \quad \widetilde{\epsilon_H} = \epsilon_H - \langle\epsilon_H\rangle_{\rm po}, \quad \widetilde{(\epsilon_H)^{1/2}} = (\epsilon_H)^{1/2} - \langle(\epsilon_H)^{1/2}\rangle_{\rm po}. \tag{38}$$

The radial displacements Δ_r of helical-ripple-trapped particles giving the main contributions to the shield of the zonal-flow potential are proportional to the radial drift velocities $\bar{v}_{\rm dr}$ of those particles and are inversely proportional to the radial electric field E_r. In helical configurations optimized for reducing neoclassical transport, helical-ripple-trapped particles have small $\bar{v}_{\rm dr}$; therefore, G_{ht} and G_h have small values, and the zonal-flow potential exhibits good response to the turbulence source. The effects of E_r on Δ_r, and accordingly on the zonal-flow response, are shown by the poloidal Mach number $M_p \equiv |(cE_r/B_0r_0)(R_0q/v_{ti})|$ in Eq. (33). Equation (33) shows that the shield of the zonal-flow potential is weakened by strengthening the radial electric field E_r and increasing M_p. For the same value of E_r, M_p can be also increased by using ions with a heavier mass, which is expected to produce zonal flows more efficiently and establish a more favorable ion-mass dependence of the ITG turbulent transport than the conventional gyro-Bohm scaling. To understand this ion-mass dependence of the zonal-flow response, we should note that the geometrical factors multiplied with M_p^{-2} represent the ratio of the neoclassical polarization $\propto(\epsilon_H)^{1/2}(k_r\Delta_r)^2$ caused by the radial drift of helical-ripple-trapped particles to the classical polarization $\propto(k_r\rho_i)^2$. This ratio becomes smaller for heavier ions because the classical polarization is proportional to the ion mass, while the neoclassical polarization is independent of the mass in the presence of the equilibrium radial electric field.

If we assume that the initial perturbed ion gyrocenter distribution function takes the Maxwellian form $\delta f^{(g)}_{i\mathbf{k}_\perp}(0) = [\delta n^{(g)}_{i\mathbf{k}_\perp}(0)/n_0]F_{i0}$ with $\delta n^{(g)}_{i\mathbf{k}_\perp}(0) = n_0(k_\perp^2\rho_{ti}^2)[e\phi_{\mathbf{k}_\perp}(0)/T_i]$ given by the quasineutrality condition, the relation of the residual zonal-flow potential at time t to its initial value is derived from Eqs. (30), (33), and (34) as

$$\phi(t) = \frac{\phi(0)}{1 + G_p + G_t + M_p^{-2}(G_{ht} + G_h)(1 + T_e/T_i)}, \tag{39}$$

where the contributions of the nonlinear source are dropped. In our earlier studies[7,8] on the zonal-flow response in helical systems without E_r, the potential shielding by helical-ripple-

trapped particles has a different dependence on $k_r\rho_{ti}$, and the residual zonal-flow potential normalized by the initial value, $\phi(t)/\phi(0)$, decreases with decreasing $k_r\rho_{ti}$. Now, Eq. (39) shows that $\phi(t)/\phi(0)$ becomes independent of $k_r\rho_{ti}$ for $k_r\rho_{ti} \ll 1$ in the presence of the poloidal $\mathbf{E}\times\mathbf{B}$ rotation of helical-ripple-trapped particles, and this result is similar to the residual zonal-flow potential obtained by Rosenbluth and Hinton for tokamaks.[3]

In the single-helicity helical configuration, where ϵ_H is independent of θ, curve C_3 coincides with C_1 in Fig. 2(a), and all helical-ripple-trapped particles exhibit poloidally closed orbits. Then, we have $G_{ht}=0$, and Eq. (40) reduces to

$$\phi(t) = \frac{\phi(0)}{1 + G_{pt} + (15/4\pi)M_p^{-2}q^2(2\epsilon_H)^{1/2}(1 + T_e/T_i)}, \quad (40)$$

where $\epsilon_T=(r_0/R_0)\cos\theta$ is used. Equation (40) corresponds to the equation derived in our previous work [note that a numerical coefficient $15/8\pi$ in Eq. (12) of Ref. 18 is corrected to $15/4\pi$ here]. In this case, $G_{pt}\equiv G_p+G_t$ coincides with the geometrical factor given by Eq. (52) in Ref. 8. Moreover, Eq. (40) agrees with the theory by Mynick and Boozer[10] in which transitions of particles between the different classes of orbits are not taken into account.

In the limit $E_r\to 0$, as in our earlier studies,[7,8] we have $|k_r\Delta_r|\to\infty$ for helical-ripple-trapped particles, and the nonadiabatic part of the helically trapped particle distribution function is damped strongly by the phase mixing due to the bounce-center radial drift. Then, the terms of the form $\langle e^{ik_r\Delta_r}\cdots\rangle_{\mathrm{po}}$ in Eqs. (27), (28), (31), and (32) vanish in helically trapped regions, and the previous results in Refs. 7 and 8 can be reproduced from Eqs. (30)–(32).

The results shown in Eqs. (33), (39), and (40) do not change when the sign of E_r is changed, because contributions of the magnetic ∇B-curvature drift velocity to the poloidal rotation are neglected compared with the $\mathbf{E}\times\mathbf{B}$ rotation. When the poloidal rotation due to the magnetic drift is added to the $\mathbf{E}\times\mathbf{B}$ rotation, the total poloidal rotation is either strengthened or weakened depending on the particle charge and class of the particle orbit. For example, in the case of $E_r>0$ and helical-rippled-trapped particles with unclosed orbits [see Fig. 2(b)], the poloidal rotation driven by the $\mathbf{E}\times\mathbf{B}$ drift is weakened by the magnetic drift for ions, while it is strengthened for electrons, although the relation between the $\mathbf{E}\times\mathbf{B}$ and magnetic poloidal drifts is reversed by changing the sign of E_r. The variation of the particle rotation speed will change the particle radial displacement and accordingly the shielding of the zonal-flow potential. The effects of the poloidal magnetic drift on the zonal-flow response are neglected in this work, although they can be included in direct numerical simulations, which may show a subtle dependence of the residual zonal flow on the sign of E_r.

V. CONCLUSIONS

In this paper, collisionless long-time behaviors of zonal flows in helical systems with radial electric fields were investigated theoretically. All classes of particles in passing, toroidally trapped, and helical-ripple-trapped states were taken into account to derive the long-time responses of the zonal-flow potential to the initial condition and turbulence source. Helical-ripple-trapped particles can exhibit either poloidally closed or unclosed orbits, and transitions from toroidally trapped orbits to unclosed orbits can occur. The effects of these transitions are also included in our theory. The resulting formulas in Eqs. (30)–(35) describe the dependencies of the long-time zonal-flow response on the helical geometry and the equilibrium radial electric field E_r. The dependence on E_r is represented by the poloidal Mach number $M_p \equiv |(cE_r/B_0r_0)(R_0q/v_t)|$. We can reduce the radial displacements of helical-ripple-trapped particles and enhance the zonal-flow response by lowering the radial drift through neoclassical optimization of the helical geometry or by boosting the poloidal rotation using a strengthened radial electric field E_r. Furthermore, under the identical conditions on the magnitude of E_r and the magnetic geometry, using ions with a heavier mass increases M_p, resulting in a higher zonal-flow response. Therefore, we can expect a more favorable ion-mass dependence of the turbulent transport than the conventional gyro-Bohm scaling.

For gyrokinetic simulation to examine the effects of the $\mathbf{E}\times\mathbf{B}$ drift of helical-ripple-trapped particles, a simulation domain must be extended from a toroidal flux tube to a poloidally global region. To confirm the validity of our theoretical predictions presented in this study, simulation studies are being conducted using the poloidally global GKV code,[19] and their results will be reported elsewhere.

ACKNOWLEDGMENTS

The authors thank Dr. M. Yokoyama for useful discussions on particle orbits in helical systems. This work is supported in part by the Japanese Ministry of Education, Culture, Sports, Science, and Technology, Grant No. 17360445, and in part by the NIFS Collaborative Research Programs, Grant Nos. NIFS08KDAD008, NIFS08KNXN145, and NIFS08KTAL006.

APPENDIX: DERIVATION OF EQUATION (27)

For passing particles and helically trapped particles having closed orbits, Eq. (27) is derived immediately using Eqs. (13) and (18), respectively, by time integration and the orbit average defined in Eq. (26). Therefore, this appendix shows the derivation of Eq. (27) only for particles undergoing a transition between toroidally trapped and helically trapped states. It should be noted that Eqs. (13) and (18) are both derived by taking an average within a helical ripple [see Eq. (7)]; therefore, $h=\bar{g}_{\mathbf{k}_\perp}$ is independent of ζ. Figure 3 shows the $(\zeta, v_\parallel)$ phase space obtained by magnifying the neighborhood of the transition point P_- [see Figs. 2(a) and 2(b)]. Here, two toroidally trapped orbits (solid curves with arrows) are seen in the $v_\parallel<0$ region. One of them is connected to a toroidally trapped orbit in the $v_\parallel>0$ region, while the other is coupled to a helically trapped orbit (a dashed curve). The latter case represents the transition from the toroidally trapped state to the helically trapped state. These two types

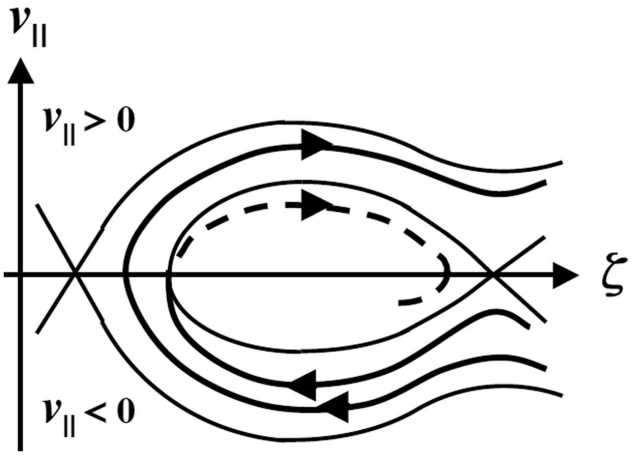

FIG. 3. The $(\zeta, v_{\|})$ phase space obtained by magnifying the neighborhood of the transition point P_-. Two toroidally trapped orbits (solid curves with arrows) are shown in the $v_{\|}<0$ region. One is connected to a toroidally trapped orbit in the $v_{\|}>0$ region while the other is coupled to a helically trapped orbit (a dashed curve with an arrow). The latter case represents the transition from the toroidally trapped state to the helically trapped state.

of particle orbits should be taken into account when we evaluate $h=\bar{g}_{\mathbf{k}_\perp}$ in the neighborhood of a transition point. For toroidally trapped particles, which do not undergo transitions to the helically trapped state but change the sign of $v_{\|}$, the boundary condition at P_- is given by

$$(g_{\mathbf{k}_\perp})_{t-} = (g_{\mathbf{k}_\perp})_{t+}, \tag{A1}$$

where the subscripts $t-$ and $t+$ represent toroidally trapped particles with $v_{\|}<0$ and $v_{\|}>0$, respectively. For particles which show transitions between the toroidally trapped and helically trapped states, we have

$$(g_{\mathbf{k}_\perp})_{t-} = (g_{\mathbf{k}_\perp})_{r}, \tag{A2}$$

where subscript r represents the helical-ripple-trapped state. It should be noted that the probability of the transition from the toroidally trapped state to the helically trapped state is given by P_t in Eq. (22). Then, $h=\bar{g}_{\mathbf{k}_\perp}$ is considered to satisfy the boundary condition expressed as

$$h_{t-} = (1-P_t)h_{t+} + P_t h_r. \tag{A3}$$

The boundary condition in Eq. (A3) at transition point P_- can also be used at P_+ [see Figs. 2(a) and 2(b)] based on an argument similar to that for the transition at P_+. Now, applying the average operation given in Eq. (24) to a combined set of Eqs. (13) and (18) and noting from Eqs. (14) and (19) that $\Delta_r=0$ at P_+ and P_-, we find from Eq. (A3) that the term $\langle \omega_\theta \partial(e^{ik_r\Delta_r}h)/\partial\theta\rangle_{\mathrm{po}}$ vanishes, and

$$\frac{\partial}{\partial t}\langle e^{ik_r\Delta_r}h\rangle_{\mathrm{po}} = \left\langle e^{ik_r\Delta_r}F_0\overline{\left(J_0\frac{e}{T}\frac{\partial\phi_{\mathbf{k}_\perp}}{\partial t}+S_{\mathbf{k}_\perp}\right)}\right\rangle_{\mathrm{po}}. \tag{A4}$$

Integrating Eq. (A4) with respect to time immediately yields Eq. (27).

[1] P. H. Diamond, S.-I. Itoh, K. Itoh, and T. S. Hahm, Plasma Phys. Controlled Fusion **47**, R35 (2005).
[2] K. Itoh, S.-I. Itoh, P. H. Diamond, A. Fujisawa, G. R. Tynan, M. Yagi, and Y. Nagashima, Phys. Plasmas **13**, 055502 (2006).
[3] M. N. Rosenbluth and F. L. Hinton, Phys. Rev. Lett. **80**, 724 (1998).
[4] Y. Xiao and P. J. Catto, Phys. Plasmas **13**, 082307 (2006).
[5] P. Angelino, X. Garbet, L. Villard, A. Bottino, S. Jolliet, Ph. Ghendrih, V. Grandgirard, B. F. McMillan, Y. Sarazin, G. Dif-Pradalier, and T. M. Tran, Phys. Plasmas **15**, 062306 (2008).
[6] Z. Gao, P. Wang, and H. Sanuki, Phys. Plasmas **15**, 074502 (2008).
[7] H. Sugama and T.-H. Watanabe, Phys. Rev. Lett. **94**, 115001 (2005).
[8] H. Sugama and T.-H. Watanabe, Phys. Plasmas **13**, 012501 (2006).
[9] S. Ferrando-Margalet, H. Sugama, and T.-H. Watanabe, Phys. Plasmas **14**, 122505 (2007).
[10] H. E. Mynick and A. H. Boozer, Phys. Plasmas **14**, 072507 (2007).
[11] A. Mishchenko, P. Helander, and A. Könies, Phys. Plasmas **15**, 072309 (2008).
[12] T. Watari, Y. Hamada, T. Notake, N. Takeuchi, and K. Itoh, Phys. Plasmas **13**, 062504 (2006).
[13] K. C. Shaing and S. A. Hokin, Phys. Fluids **26**, 2136 (1983).
[14] M. Wakatani, *Stellarator and Heliotron Devices* (Oxford University Press, Oxford, 1998), Chaps. 6 and 7.
[15] H. Sugama and S. Nishimura, Phys. Plasmas **9**, 4637 (2002); H. Sugama and T.-H. Watanabe, *ibid.* **15**, 042502 (2008).
[16] T.-H. Watanabe, H. Sugama, and S. Ferrando-Margalet, Nucl. Fusion **47**, 1383 (2007).
[17] T.-H. Watanabe, H. Sugama, and S. Ferrando-Margalet, Phys. Rev. Lett. **100**, 195002 (2008).
[18] H. Sugama, T.-H. Watanabe, and S. Ferrando-Margalet, J. Plasma Fusion Res. **3**, 041 (2008).
[19] T.-H. Watanabe, H. Sugama, and S. Ferrando-Margalet, *Proceedings of the 22nd IAEA Fusion Energy Conference*, Geneva, Switzerland, 2008 (IAEA, Vienna, 2008), Paper No. TH/P8-20.
[20] O. Motojima, N. Ohyabu, A. Komori, O. Kaneko, H. Yamada, K. Kawahata, Y. Nakamura, K. Ida, T. Akiyama, N. Ashikawa, W. A. Cooper, A. Ejiri, M. Emoto, N. Ezumi, H. Funaba, A. Fukuyama, P. Goncharov, M. Goto, H. Idei, K. Ikeda, S. Inagaki, M. Isobe, S. Kado, H. Kawazome, K. Khlopenkov, T. Kobuchi, K. Kondo, A. Kostrioukov, S. Kubo, R. Kumazawa, Y. Liang, J. F. Lyon, A. Mase, S. Masuzaki, T. Minami, J. Miyazawa, T. Morisaki, S. Morita, S. Murakami, S. Muto, T. Mutoh, K. Nagaoka, Y. Nagayama, N. Nakajima, K. Nakamura, H. Nakanishi, K. Narihara, Y. Narushima, K. Nishimura, N. Nishino, N. Noda, T. Notake, H. Nozato, S. Ohdachi, Y. Oka, H. Okada, S. Okamura, M. Osakabe, T. Ozaki, B. J. Peterson, A. Sagara, T. Saida, K. Saito, S. Sakakibara, M. Sakamoto, R. Sakamoto, M. Sasao, K. Sato, M. Sato, T. Seki, T. Shimozuma, M. Shoji, H. Suzuki, Y. Takeiri, N. Takeuchi, N. Tamura, K. Tanaka, M. Y. Tanaka, Y. Teramachi, K. Toi, T. Tokuzawa, Y. Tomota, Y. Torii, K. Tsumori, K. Y. Watanabe, T. Watari, Y. Xu, I. Yamada, S. Yamamoto, T. Yamamoto, M. Yokoyama, S. Yoshimura, Y. Yoshimura, M. Yoshinuma, N. Asakura, T. Fujita, T. Fukuda, T. Hatae, S. Higashijima, A. Isayama, Y. Kamada, H. Kubo, Y. Kusama, Y. Miura, T. Nakano, H. Ninomiya, T. Oikawa, N. Oyama, Y. Sakamoto, K. Shinohara, T. Suzuki, H. Takenaga, K. Ushigusa, T. Hino, M. Ichimura, Y. Takase, F. Sano, H. Zushi, T. Satow, S. Imagawa, T. Mito, I. Ohtake, T. Uda, K. Itoh, K. Ohkubo, S. Sudo, K. Yamazaki, K. Matsuoka, Y. Hamada, and M. Fujiwara, Nucl. Fusion **43**, 1674 (2003).
[21] H. Yamada, A. Komori, N. Ohyabu, O. Kaneko, K. Kawahata, K.-Y. Watanabe, S. Sakakibara, S. Murakami, K. Ida, R. Sakamoto, Y. Liang, J. Miyazawa, K. Tanaka, Y. Narushima, S. Morita, S. Masuzaki, T. Morisaki, N. Ashikawa, L. R. Baylor, W. A. Cooper, M. Emoto, P. W. Fisher, H. Funaba, M. Goto, H. Idei, K. Ikeda, S. Inagaki, N. Inoue, M. Isobe, K. Khlopenkov, T. Kobuchi, A. Kostrioukov, S. Kubo, T. Kuroda, R. Kumazawa, T. Minami, S. Muto, T. Mutoh, Y. Nagayama, N. Nakajima, Y. Nakamura, H. Nakanishi, K. Narihara, K. Nishimura, N. Noda, T. Notake, S. Ohdachi, Y. Oka, M. Osakabe, T. Ozaki, B. J. Peterson, G. Rewoldt, A. Sagara, K. Saito, H. Sasao, M. Sasao, K. Sato, M. Sato, T. Seki, H. Sugama, T. Shimozuma, M. Shoji, H. Suzuki, Y. Takeiri, N. Tamura, K. Toi, T. Tokuzawa, Y. Torii, K. Tsumori, T. Watanabe, I. Yamada, S. Yamamoto, M. Yokoyama, Y. Yoshimura, T. Watari, Y. Xu, K. Itoh, K. Matsuoka, K. Ohkubo, T. Satow, S. Sudo, T. Uda, K. Yamazaki, O. Motojima, and M. Fujiwara, Plasma Phys. Controlled Fusion **43**, A55 (2001).
[22] M. Yokoyama, J. Plasma Fusion Res. **78**, 205 (2002).
[23] H. E. Mynick, Phys. Plasmas **13**, 058102 (2006).
[24] D. A. Spong, S. P. Hirshman, L. A. Berry, J. F. Lyon, R. H. Fowler, D. J. Strickler, M. J. Cole, B. N. Nelson, D. E. Williamson, A. S. Ware, D. Alban, R. Sánchez, G. Y. Fu, D. A. Monticello, W. H. Miner, and P. M. Valanju, Nucl. Fusion **41**, 711 (2001).

[25]J. N. Talmadge, V. Sakaguchi, F. S. B. Anderson, D. T. Anderson, and A. F. Almagri, Phys. Plasmas **8**, 5165 (2001).
[26]G. Grieger, W. Lotz, P. Merkel, J. Nührenberg, J. Sapper, E. Strumberger, H. Wobig, R. Burhenn, V. Erckmann, U. Gasparino, L. Giannone, H. J. Hartfuss, R. Jaenicke, G. Kühner, H. Ringler, A. Weller, and F. Wagner, Phys. Fluids B **4**, 2081 (1992).
[27]J. R. Cary, C. L. Hedrick, and J. S. Tolliver, Phys. Fluids **31**, 1586 (1988).
[28]W. Horton, Rev. Mod. Phys. **71**, 735 (1999).
[29]E. A. Frieman and L. Chen, Phys. Fluids **25**, 502 (1982).
[30]R. D. Hazeltine and J. D. Meiss, *Plasma Confinement* (Addison-Wesley, Redwood, 1992), p. 298.